

# 1 Performance of a passive acoustic 2 linear array in a tidal channel

3 Matthew F. Auvinen, David R. Barclay

4 **Abstract**

5 Baseline ambient sound level assessment is important in quantifying anthropogenic noise contributions. Static  
6 acoustic sensing in high-flow conditions is complicated by pseudo-sound, or flow noise, caused by turbulent flow  
7 on the surface of a hydrophone. Signal processing methods are used to identify and suppress flow noise at low  
8 frequencies (< 500 Hz) in data collected on a four-element horizontal hydrophone array in Minas Passage, a tidal  
9 channel in the Bay of Fundy, in October 2016. Spectral slope analysis is used to identify the frequencies at which  
10 the flow noise and ambient noise contributions to the recorded signal are equal. The maximum frequencies at  
11 which flow noise is observed is determined using analysis of the spatial coherence. The array's performance in the  
12 Minas Passage is quantified by an empirical relationship between flow speed and the spectral critical frequencies  
13 of the coherent output from the linear array. Coherent averaging (broadside beamforming) is demonstrated as an  
14 effective flow noise suppression technique, improving low-frequency passive acoustic monitoring in a high-energy  
15 tidal channel.

16 **Index Terms**

17 Flow noise, ambient noise, array processing, tidal channel, and passive acoustic monitoring.

18 **I. INTRODUCTION**

19 **T**IDAL power utilities are currently leasing seafloor space within the Minas Passage in the Bay of  
20 Fundy with aspirations of converting the energy of the region's tidal currents into electricity, a  
21 trend that has been supported by favorable projections of the Passage's tidal energy capacity [1]. It is  
22 important that these companies follow sustainable industry practices as the sector grows. This includes the

Dr. David Barclay is an assistant professor in the Department of Oceanography, Dalhousie University. Matthew Auvinen holds a B.Sc. (Hons) from the Department of Oceanography, Dalhousie University, Halifax, NS (email: matthewauvinen@gmail.com; dbarclay@dal.ca).

Manuscript received June 26, 2017; revised MONTTH XX, 201X. This work was supported by the Natural Sciences and Engineering Research Council of Canada, GeoSpectrum Technologies, and Black Rock Tidal Power.

23 consideration of industry knowledge gaps, many of which are a consequence of the sector's immaturity [2].  
24 The uncertainty surrounding the ecological and environmental implications of tidal turbine infrastructure  
25 is a particularly important knowledge gap and has qualified some opposition to turbine projects.

26 Tidal turbines present two environmental concerns: physical contact (or interaction) with marine life  
27 [3] [4] and acoustic pollution. Tidal turbines could become an important source of ambient noise in  
28 tidal channels through cavitation and motor or mechanical noise [5]. Turbine anthropophony could affect  
29 animal navigation, communication, predator-prey detections [6], and marine life cycles [7]. Moreover,  
30 turbine-generated sound could be damaging to fish tissue [8]. If substantive, these effects would threaten  
31 near-field and far-field ecosystem health, stressing the need for rigorous environmental impact assessments  
32 in the tidal power sector.

33 These environmental risks emphasize the need for baseline ambient noise measurements in the Minas  
34 Passage, against which turbine noise pollution will be measured. However, the utility of ambient sensing  
35 is limited by pseudo-sound, or flow noise, generated on the surface of a hydrophone in turbulent water.  
36 Indeed, the masking effects of flow noise can complicate source identification and background noise  
37 assessment in high-flow settings, such as tidal channels.

38 Analogous to turbulent flowing air [9], flowing water in a high Reynolds number regime generates  
39 pressure fluctuations on the surface of a hydrophone. These pressure fluctuations produce flow noise  
40 which is irregular, uncorrelated, and random. Local pressure fluctuations on the surface of a hydrophone  
41 represent near-field turbulence [10]. Free-drifting hydrophones moving with the mean water flow will  
42 experience little signal contamination, as it is the relative flow of water over a hydrophone's surface that  
43 leads to flow noise.

44 Turbulent flows occupy a wide range of frequencies and wavenumber domains, with broad spatial and  
45 temporal variability. The advective nonlinearity of turbulent flows makes them unpredictable in space  
46 and time, and contributes to their complex nature [11]. As such, it is difficult to reliably model flow  
47 noise. Flow noise follows a spectral slope of  $f^{-5/3}$  at low frequencies, behaviour that is analogous by  
48 Kolmogorov's turbulence theory. This flow noise is not to be confused with wind-generated noise that  
49 produces  $f^{-5/3}$  spectral slopes at higher frequencies [12]. Bassett et al. [13] identifies  $f^{-5/3}$  flow noise  
50 below 20 Hz and also describes steepened spectral slopes,  $f^{-m}$ , between 20 and 200 Hz. Lombardi [6]  
51 identifies these steep spectral slopes in measurements from the Grand Passage tidal channel. The flow  
52 noise that produces  $f^{-m}$  is a result of small-scale turbulence being averaged out across the surface of the

53 hydrophones, which dampens (or reduces) measurements.

54 Flow noise presents a unique challenge for passive acoustic monitoring (PAM): a hydrophone in a  
55 high-flow setting will record both propagating sound and pseudo-sound. This suggests that models should  
56 distinguish between the two sound sources. Barclay and Buckingham [14] describe the exploitation of  
57 ambient noise coherence and cross-correlation to address flow noise in deep sea signals. We adapt this  
58 application of coherence to identify and suppress flow noise across a four-element array in a tidal channel.

59 Successful suppression of flow noise could benefit PAM systems in relatively energetic environments.

60 The objectives of the present research are:

61 1) Use spectral analysis and spatial coherence to identify and characterize flow noise at low frequencies  
62 ( $< 500$  Hz).

63 2) Use coherent averaging (beamforming) to improve the performance of a linear hydrophone array  
64 by suppressing flow noise and enhancing the measurement of ambient noise.

65 This paper is organized as follows. Section II discusses important field work details, including an  
66 experiment description and instrumentation summary. Section III describes all relevant signal processing,  
67 with emphasis on spectral analysis, spatial coherence, and beamforming. Section IV presents the signal  
68 processing and data analysis results. Section V evaluates the results and identifies areas for future work.

69 Lastly, Section VI summarizes the findings of the study in a series of conclusions.

## 70 II. FIELD WORK

71 Field work was completed on October 27, 2016, near the Fundy Ocean Research Center for Energy  
72 (FORCE) site in the Minas Passage of the Bay of Fundy. The FORCE site depth ranges between 40 and  
73 60 meters depending on the tide. The deployment period spanned roughly four hours, from 12:00 ADT  
74 to 16:00 ADT. This experimental window captured the transition from ebb tide to slack tide. Wind speed  
75 was measured intermittently throughout the deployment period using a hand-held wind speed gauge. Tidal  
76 and flow data was generated using a WebTide model [15].

77 There is a substantial fish population in the Minas Passage [3], some of which could contribute  
78 to the local ambient sound field [16]. Pilot whales, dolphins, seals, and other marine mammals that  
79 frequent the Minas Passage are another potential source of ambient noise. These animals generate sound  
80 through a variety of mechanisms, such as muscle action, stridulation, and vocalization [17]. Non-biological  
81 sound sources in the Minas Passage include wave action, anthropogenic activity, and bubbles. Proper

82 characterization of the local sound field at the FORCE site would require consideration these potential  
83 sound sources. However, their variability makes source identification challenging.

84 *A. Experiment*

85 A linear hydrophone array was streamed behind the *MV Nova Endeavour* (42' x 16'), which was  
86 anchored to the seafloor of the Minas Passage while in dead ship. The array was positioned roughly 15  
87 meters below the sea surface using a towfish depressor. The strength of the current kept the array at a  
88 relatively constant depth. Four hydrophones were simultaneously sampled over a four hour period and  
89 processed by an analog-to-digital converter (ADC) on board the *MV Nova Endeavour*. The signal cable,  
90 which carried both the array and a drogue, was sheathed in a fairing to reduce strum generation and  
91 attached to a tow cable (6GA galvanized wire) using cable ties.

92 A drifting hydrophone (Geospectrum Technologies GuardBuoy) was deployed using a small auxiliary  
93 vessel launched from the *MV Nova Endeavour*. The GuardBuoy was suspended 2 meters below the surface  
94 using a drifting surface float and isolation system made of a damping mass and a Dacron non-stretch line  
95 and compliant bungee. The system isolated the recording hydrophone and instrument package from any  
96 surface action, such as the vertical movement of waves, which would otherwise generate mechanical or  
97 flow noise.

98 A total of five transects were performed by driving the GuardBuoy upstream in a rigid-hulled inflatable  
99 boat (RHIB), deploying the drifter, turning off the RHIB engines, and then floating downstream with at  
100 least 15 meters between the RHIB and the GuardBuoy. The GuardBuoy and RHIB followed a downstream  
101 transect that passed over the array. The GuardBuoy was retrieved once it had reached 20 meters beyond  
102 the array. These transects were performed over the course of three hours, beginning at 13:00 ADT. The  
103 GuardBuoy signals are assumed to be free of flow noise and were used as benchmarks to assess the  
104 performance of the array. The turbulent tidal channel is assumed to be well mixed with an isovelocity  
105 sound speed profile, minimizing noise field variability over the depth difference between the two systems.

106 *B. Instrumentation*

107 The linear array is an oil-filled array with a rigid exterior and acoustically transparent outer skin.  
108 It contains four sequentially spaced hydrophones with a horizontal configuration along the axis of the  
109 array. The array and the hydrophones were constructed by GeoSpectrum Technologies. Each neighbouring  
110 hydrophone is separated by a distance  $d = 17\text{cm}$ . The array hydrophones were set to simultaneously sample

111 at a rate of 96 kHz with an acoustic bandwidth of 48.019 kHz. The four channels on the array continuously  
 112 recorded 10 minute WAV files over a 4 hour period. Power spectra were calibrated to dB re 1  $\mu$ Pa according  
 113 to frequency-dependent sensitivities supplied by the manufacturer. The GuardBuoy sampled at a rate of  
 114 96 kHz with an acoustic bandwidth of 48 kHz, and was equipped with a GPS to record transect geospatial  
 115 information. The Guard Buoy recorded WAV files in 30 minute segments. Corresponding power spectra  
 116 were converted to dB re 1  $\mu$ Pa according to frequency-dependent sensitivities supplied by the manufacturer.

### 117 III. DATA ANALYSIS

118 Data analysis was performed in MATLAB in several stages. The analysis began with the calculation of  
 119 the power spectral density (PSD) from the raw WAV files, followed by spectral analysis, spatial coherence  
 120 analysis, and broadside beamforming.

121 *A. General Signal Processing*

The output of a hydrophone is defined as

$$x_i(t) = \sigma_i(t) + n_i(t) \quad (1)$$

122 where  $x_i$  is the recorded time series on each  $i$ th hydrophone,  $\sigma_i$  is the sound field's ambient components,  
 123 and  $n_i$  is the locally generated flow noise. Importantly,  $n_i$  and  $\sigma_i$  are uncorrelated. Furthermore, the  
 124 inherent randomness of flow noise makes  $n_i$  incoherent with respect to  $n_j$ .

125 The power spectrum, or spectral density, is defined as

$$S_{ii}(\omega) = \frac{\langle X_i(\omega) \cdot X_i^*(\omega) \rangle}{T} \quad (2)$$

126 where  $X_i$  is the Fourier transform of  $x_i$ ,  $\omega$  is angular frequency,  $*$  denotes a complex conjugate,  $\langle \rangle$   
 127 indicates an ensemble average, and  $T$  is the observation interval. All Fourier transforms are windowed  
 128 by a Hann function. The Hann function's effect on the variance has been accounted for. The time series  
 129 were divided into 34.1 second-long segments, where each segment was further split into 50 contiguous  
 130 subsegments of 0.682s with no overlap. A  $2^{16}$  Fourier transform was applied to each subsegment, from  
 131 which ensemble averaging produced a power spectral density with a frequency bin width of 1.47 Hz.  
 132 Coherence is used to quantify the similarity between two signals and is defined as

$$\Gamma_{ij}(\omega) = \frac{S_{ij}(\omega)}{(S_{ii}(\omega) \cdot S_{jj}(\omega))^{\frac{1}{2}}}. \quad (3)$$

133 **B. Power Spectrum Probability Density**

134 Spectral probability density (SPD) is an analytical technique used to depict the variability of the power  
 135 spectrum over a period that is much longer than the minimum time required for a stationary measurement  
 136 of power to be made [18]. This form of analysis facilitates the identification of unique events within a  
 137 series of spectra. The power spectrum probability density (PSPD) is defined as

$$\text{PSPD}(f) = H(S_{ii}(f), h) \quad (4)$$

138 where  $\text{PSPD}(f)$  is the power spectrum probability density at frequency  $f$ , and  $H(S(f), h)$  is the histogram  
 139 of the power spectrum  $S_{ii}$  at frequency  $f$  with a histogram bin width of  $h$  dB re  $1 \mu\text{Pa}^2/\text{Hz}$ . By combining  
 140 PSPD results across frequencies, we generate a PSPD matrix

$$\begin{bmatrix} \text{PSPD}(f_1) & \text{PSPD}(f_2) & \text{PSPD}(f_3) & \dots & \text{PSPD}(f_a) \end{bmatrix} \quad (5)$$

141 where  $\text{PSPD}(f_a)$  is the PSPD at the  $a$ th frequency.

142 **C. Spectral Critical Frequency**

143 Lombardi [6] and Bassett et al. [13] suggest that there are three distinct spectral slope regions in  
 144 the low-to-mid-frequency range: spectral slopes of Kolmogorov's  $f^{-5/3}$ ; steepened flow noise spectral  
 145 slopes,  $f^{-m}$ , that include the effects of a finite volume sensor [13]; and an ambient noise region that is  
 146 determined by near-field and far-field ambient sound sources.

The local spectral slope is defined as

$$-M = \frac{S_{ii}(2\pi f_a) - S_{ii}(2\pi f_b)}{\log(f_a \cdot f_b^{-1})} \quad (6)$$

147 where  $S_{ii}(2\pi f_a)$  is the spectral density on the  $i$ th sensor at frequency  $f_a$  and  $S_{ii}(2\pi f_b)$  is the spectral  
 148 density on the  $i$ th sensor at frequency  $f_b$ . (6) describes the spectral slope in dB/decade.

149 The transition from the flow noise region of  $f^{-m}$  to the ambient noise region is marked by the frequency  
 150 knee, where the spectral slope begins to shallow. That is, the exit from the flow noise region is marked by

151 a deviation below the slope  $f^{-m}$ . Here, the spectral critical frequency,  $f_c$ , is defined as the first frequency  
 152 at which

$$|M| < |m| \quad (7)$$

153 is true. Importantly, both slopes in (7) are in dB/decade.

154 *D. Coherence Critical Frequency*

155 Spatial coherence is calculated for each channel combination using (3), providing an assessment of  
 156 signal similarity between elements. Propagating ambient noise is highly correlated across the array.  
 157 Additionally, propagating noise at wavelengths sufficiently large relative to element spacing produces  
 158 very high coherence at low frequencies by effectively co-locating sensors. Conversely, flow noise is a  
 159 source of incoherence, as pseudo-sound is uncorrelated across the linear array (when turbulent scales are  
 160 lesser than hydrophone separation). Therefore, in the band  $f < 500$  Hz, flow noise is marked by low  
 161 coherence while ambient noise is marked by high coherence. The transit of this coherence boundary, from  
 162 flow noise (incoherent) to ambient noise (coherent) provides a metric for describing the extent of flow  
 163 noise across the array.

164 The coherence critical frequency,  $f'_c$ , is defined as the frequency at which a minimum coherence  
 165 threshold is crossed due to flow noise masking. To establish this coherence threshold, we assume an  
 166 isotropic ambient noise field such that the horizontal coherence is given by Buckingham [19]

$$G_{ij}(\omega') = \frac{\sin(\omega'_{ij})}{\omega'_{ij}} \quad (8)$$

167 where

$$\omega'_{ij} = \frac{2\pi d_{ij} f}{c}. \quad (9)$$

168 Here,  $d_{ij}$  is the separation distance between the  $i$ th and  $j$ th hydrophone and  $c$  is the local sound speed.  
 169 We define  $f'_c$  as the first frequency at which

$$|\Gamma_{ij}(\omega')| \geq 0.9 \cdot G_{ij}(\omega') \quad (10)$$

is true. We can be confident that any coherence within 10% of (8) is real and significant while any drop below the threshold given by the right hand side of (10) is caused by the addition of flow-generated incoherent noise. This automated critical frequency detector corresponds to a coherence threshold of  $\sim 0.9$ . The use of a more sophisticated noise model such as Cron and Sherman [20] or Deane et al. [21] in the place of (8) yields a nearly identical threshold.

### 175 E. Linear Regression

176 Least squared linear regressions between critical frequencies,  $f_c$  and  $f'_c$ , and flow speed,  $u$ , are used to  
 177 identify and characterize the prevalence of flow noise and ambient noise in measurements. No data points  
 178 are excluded from these regressions.

### 179 F. Beamforming

180 We use a broadside beamformer to coherently average the channels across the array. Locally generated  
 181 flow noise and the ambient sound field are inseparable, however we can describe their relative prevalence  
 182 with the theoretical signal-noise ratio (SNR) where we are defining ambient sound as the signal, and flow  
 183 noise as the noise. By taking the Fourier transform of (1) and substituting into (2), we find

$$S_{ii} = \frac{\langle (\varsigma_i + N_i) \cdot (\varsigma_i^* + N_i^*) \rangle}{T} \quad (11)$$

184 where  $\varsigma_i$  and  $N_i$  are the Fourier transforms of  $\sigma_i$  and  $n_i$ , respectively. For clarity, the frequency dependency  
 185 has been omitted. Since  $\varsigma_i$  and  $N_i$  are uncorrelated, we can expand (11) to arrive at

$$S_{ii} = \frac{\langle \varsigma_i \varsigma_i^* \rangle + \langle N_i N_i^* \rangle}{T}. \quad (12)$$

186 Given (12), the SNR for a single hydrophone ( $\text{SNR}_H$ ) is defined as

$$\text{SNR}_H = \frac{\langle \varsigma_i \varsigma_i^* \rangle}{\langle N_i N_i^* \rangle} \quad (13)$$

187 where  $\text{SNR}_H = 1$  at the critical frequency,  $f_c$ . Now consider an array of hydrophones indexed by  $i$ , where  
 188 the ambient sound field component of the signal on each phone is

$$\sigma_{i+1}(t) = \sigma_1(t - \tau_i) \quad (i > 1) \quad (14)$$

189 where

$$\tau_i = \frac{i \cdot d \cos \theta}{c} \quad (15)$$

190 is the acoustic travel time in seconds for plane wave noise arriving on the sensors at the angle  $\theta$ . Here,  
 191  $d$  is the nearest neighbour element separation. Taking the Fourier transform of (14) gives

$$\varsigma_i(\omega) = \varsigma_1(\omega) e^{-i\omega\tau_i}. \quad (16)$$

192 The coherent sum of the signals across the array is defined as

$$x_T(t) = \sum_{i=1}^l x_i(t) \quad (17)$$

193 where  $x_i(t)$  is the signal recorded on the  $i$ th element of a linear array  $l$  elements long. Since no time  
 194 delay has been applied to  $x_i(t)$ ,  $x_T(t)$  is the equivalent to beamforming broadside to the array. Since the  
 195 source of interest is ambient noise, the sound field is assumed to be axially symmetric. Thus the horizontal  
 196 array orientation and beam direction are unimportant, provided an appropriate array gain compensation  
 197 is applied.

198 The Fourier transform of (17) is

$$X_T(\omega) = \sum_{i=1}^l X_i(\omega). \quad (18)$$

<sup>199</sup> The array power spectral density can be estimated using (18) by

$$A = \frac{\langle X_T(\omega) \cdot X_T^*(\omega) \rangle}{T}. \quad (19)$$

<sup>200</sup> Given an array with both ambient noise and flow noise components, (18) can be expanded to

$$X_T = [\varsigma_1 + N_1 + \varsigma_2 + N_2 + \dots + \varsigma_l + N_l] \quad (20)$$

<sup>201</sup> which describes the total output of all sensors on an array with  $l$  elements. Substituting (16) into (20)  
<sup>202</sup> gives

$$X_T = \varsigma_1 + N_1 + \sum_{i=1}^l (\varsigma_i e^{-i\omega\tau_i} + N_{i+1}). \quad (21)$$

<sup>203</sup> Using the Fourier transform of the coherently summed outputs across the array, the power spectral density  
<sup>204</sup> can be computed by substituting (21) into (19) yielding

$$A = \frac{\langle \varsigma_1 \varsigma_1^* \left[ l + \sum_{i=1}^{l-1} \frac{1}{2} (l-i) \cos(\omega\tau_i) \right] + N \cdot N^* \rangle}{T} \quad (22)$$

<sup>205</sup> where

$$N = \sum_i^l N_i \quad (23)$$

<sup>206</sup> is the coherently summed flow noise. This term can be simplified by assuming the power of the flow  
<sup>207</sup> noise measured on each individual hydrophone is equal across the array,

$$\langle N_i N_i^* \rangle = \langle N_j N_j^* \rangle \quad (24)$$

<sup>208</sup> and uncorrelated between the sensors,

$$\langle N_i N_j^* \rangle = \delta_{ij} \cdot N_1 N_1^* \quad (25)$$

<sup>209</sup>

$$\delta_{ij} = \begin{cases} 0 & \text{if } i \neq j \\ 1 & \text{if } i = j. \end{cases}$$

<sup>210</sup> Then the total power received by the array becomes

$$A = \frac{\langle \zeta_1 \zeta_1^* \rangle \left[ l + \sum_{i=1}^{l-1} \frac{1}{2} (l-i) \cos(\omega \tau_i) \right] + l \langle N_1 N_1^* \rangle}{T}. \quad (26)$$

<sup>211</sup> Furthermore, if  $K$  is defined as

$$K = l + \sum_{i=1}^{l-1} \frac{1}{2} (l-i) \cos(\omega \tau_i) \quad (27)$$

<sup>212</sup> then (26) becomes

$$A = \frac{K \langle \zeta_1 \zeta_1^* \rangle + l \langle N_1 N_1^* \rangle}{T} \quad (28)$$

<sup>213</sup> where (28) describes the array spectral density. Here,  $SNR_A$  describes the relative strength of the ambient  
<sup>214</sup> noise and flow noise components of the array output, such that

$$SNR_A = \frac{K \langle \zeta_1 \zeta_1^* \rangle}{l \langle N_1 N_1^* \rangle}. \quad (29)$$

<sup>215</sup> Comparing (29) to the result derived for a single hydrophone, given by (13), we see that the beamformed  
<sup>216</sup> array improves the signal-to-noise ratio by a factor of  $\frac{K}{l}$ . Furthermore, (29) suggests that array performance

improves with an increasing number of hydrophones,  $l$ . For an array with 4 elements, at broadside,  $\frac{K}{l} = \frac{7}{4}$ .

### 219 G. Array Gain

220 The broadside beamforming analysis applied to the linear array generates artificial spectral density gain.  
 221 As a result, an array gain formula is applied to the beamformed results to correct the inflated values. The  
 222 array gain formula presented here is adapted from Cox [22], such that

$$AG = 10 \log l. \quad (30)$$

223 The array gain correction is performed by subtracting the result of (30) from the calculated array power  
 224 spectral density.

### 225 H. Algorithm Assessment

226 All channel signals are consolidated into one coherent array output using (18) and (19). The resulting  
 227 coherent array signal is compared to signals from the GuardBuoy and a single fixed hydrophone to evaluate  
 228 the performance of the beamformed array. The algorithm is further tested by comparing the coherent array  
 229 spectral critical frequencies to the spectral critical frequencies of a fixed single hydrophone.

## 230 IV. RESULTS

### 231 A. Spectral Density

232 A comparison between spectral density and current speed (Fig. 1) reveals high signal levels in fast  
 233 flowing water and low signal levels in slow flowing water. The signal power is high below 10 Hz and falls  
 234 off as the frequency approaches 100 Hz, which indicates that flow noise is prevalent at low frequencies.

235 The hydrophone power spectrum contains multiple episodes of mid-frequency noise. These signals are  
 236 attributed to ship noise generated by passing ships and the small vessel used in the GuardBuoy drifter  
 237 tests. The abrupt shift in spectral density at 90 minutes is attributed to a reset of the ground between the  
 238 data acquisition hardware and the array housing. The data collected during the reset have been omitted.

239 *B. Power Spectrum Probability Density*

240 The PSPD ( Fig. 2) facilitates the broad-scale assessment of a hydrophone's spectral density over entire  
241 deployment periods. The PSPD follows a spectral slope of  $f^{-5/3}$  below 10 Hz, behaviour analogous to  
242 Kolmogorov's turbulence theory. This spectral slope marks a region of flow noise within the signal. A  
243 steepened spectral slope of  $f^{-m}$ , where  $m > \frac{5}{3}$ , persists between 40 and 100 Hz, a result of small-scale  
244 turbulence when turbulence wavelength  $\ll$  sensor size. This small-scale turbulence is averaged out over  
245 the surface of the hydrophone sensor, dampening the measured signals. The PSPD results show that  
246 ambient noise is dominant above 300 Hz, where signal levels are markedly low. Single power spectra are  
247 superimposed on the PSPD and suggest that measurements in slow current conditions contain a greater  
248 extent of ambient noise relative to those in fast current conditions.

249 Early in the deployment (around 10 minutes) electronic noise in the system raised the noise floor to 90  
250 dB  $\mu$ Pa. While this was quickly remedied on site and has been accounted for in the data, a noise floor  
251 persisted around 60 dB  $\mu$ Pa.

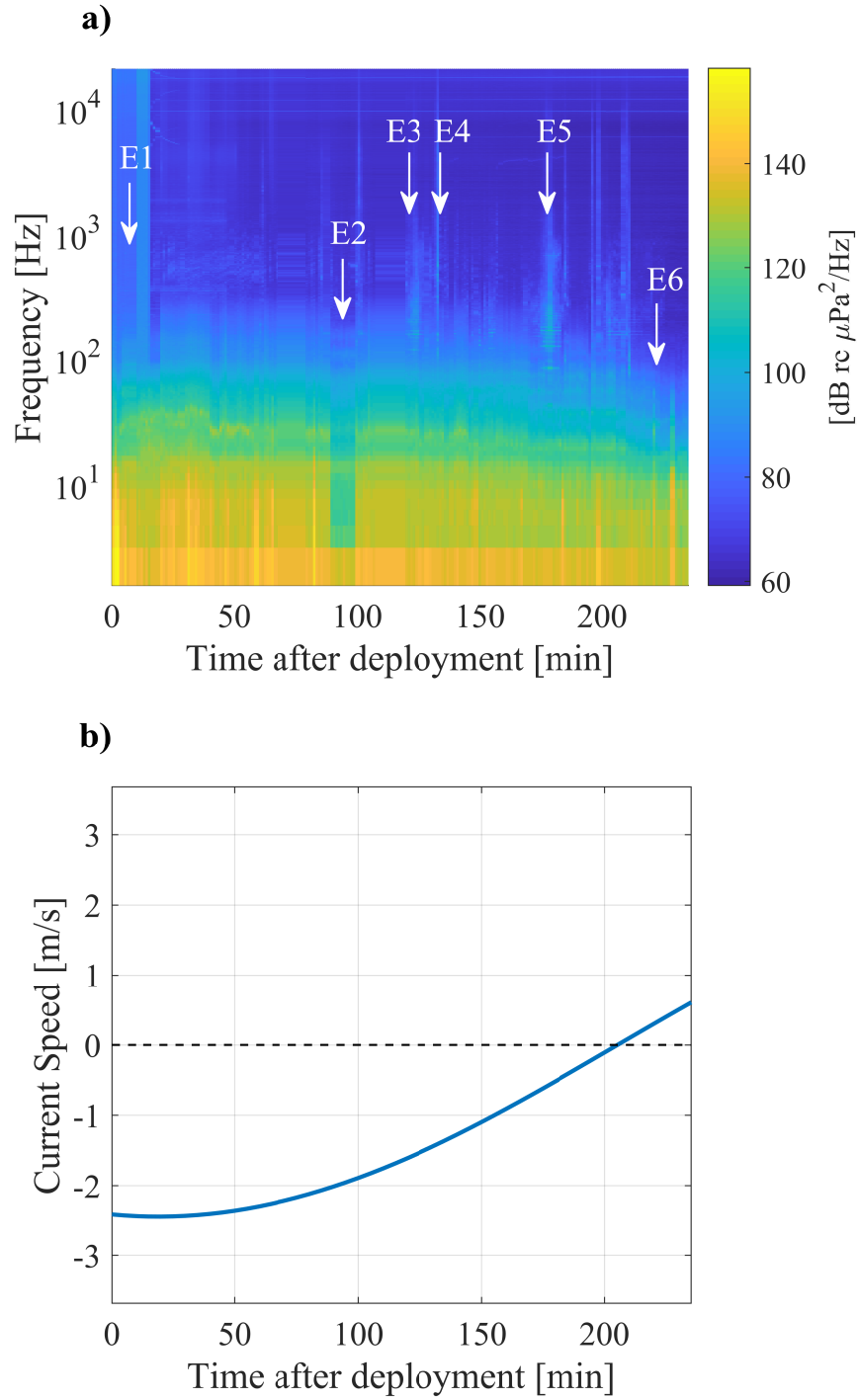


Fig. 1. Power spectrum for channel 0 on the array (a). The spectrum is plotted over the deployment period across a range of low-to-mid frequencies. Different mid-frequency noise events are represented by E1 - E6. The spectrum begins at maximum ebb tide and ends shortly after slack tide, as shown by the current speed time series (b). Power decreases with current speed over the deployment period.

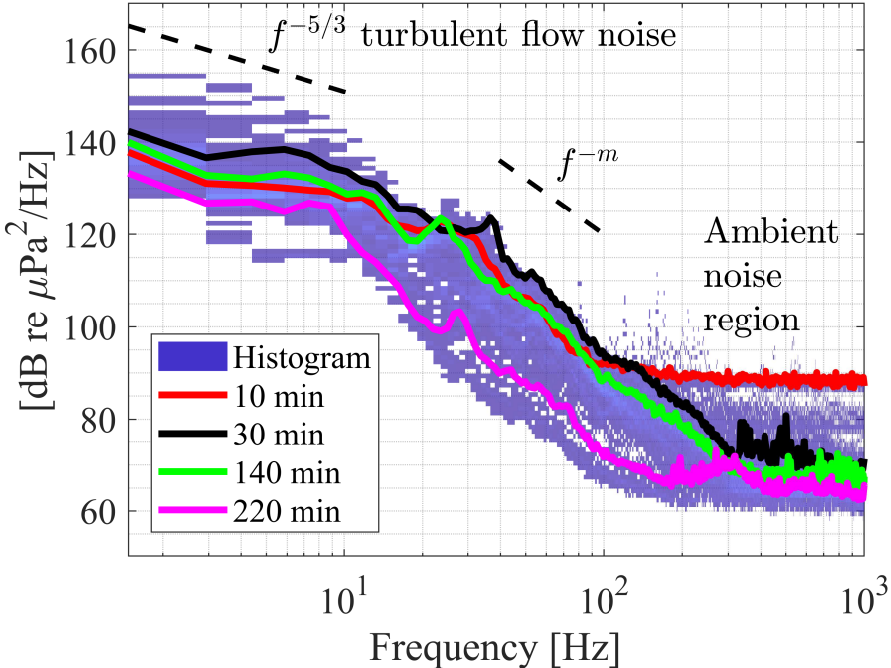


Fig. 2. Fixed single hydrophone power spectrum probability density over the entire deployment period. Turbulent flow noise is prevalent  $< 10$  Hz (where wavelengths  $\gg$  sensor size), with a spectral slope of  $f^{-5/3}$ , while turbulence interacting with the hydrophone's finite volume (in the 10 Hz to 100 Hz band) yields a spectral slope of  $f^{-m}$ . The ambient sound field dominates at frequencies  $> 300$  Hz. Coloured lines represent individual spectra recorded at the time after deployment indicated in the legend.

### 252 C. Spectral Critical Frequency

253 Spectral slopes were calculated between 40 and 100 Hz for each minute of deployment using (6). The  
 254 linear relationship between spectral slope,  $m$ , and current speed,  $u$ , (Fig. 3) indicates that signals recorded  
 255 in decreasing flow are increasingly damped (steepened slope). The inverse relationship between current  
 256 speed and spectral slope suggests that signals are less damped in fast flowing water, a result of larger  
 257 turbulence scales. The spectral slopes observed between 40 and 100 Hz range from -25 to -60 dB/decade.  
 258 The correlation coefficient,  $R$ , indicates that there is a meaningful correlation between spectral slope and  
 259 current.

260 The spectral critical frequency was calculated for each minute of deployment using (7). These critical  
 261 frequencies were regressed against current speed, as shown in Fig. 4. There is a positive correlation  
 262 between spectral critical frequency and current speed, where fast flow coincides with high spectral critical  
 263 frequencies. The spectral critical frequency is the frequency at which flow noise and ambient noise are  
 264 equal in power.

265 The intercepts have not been forced to zero. This is because it is unrealistic to expect that we can com-  
 266 pletely eliminate flow noise, or low-frequency noise generated by the mechanical systems that comprise

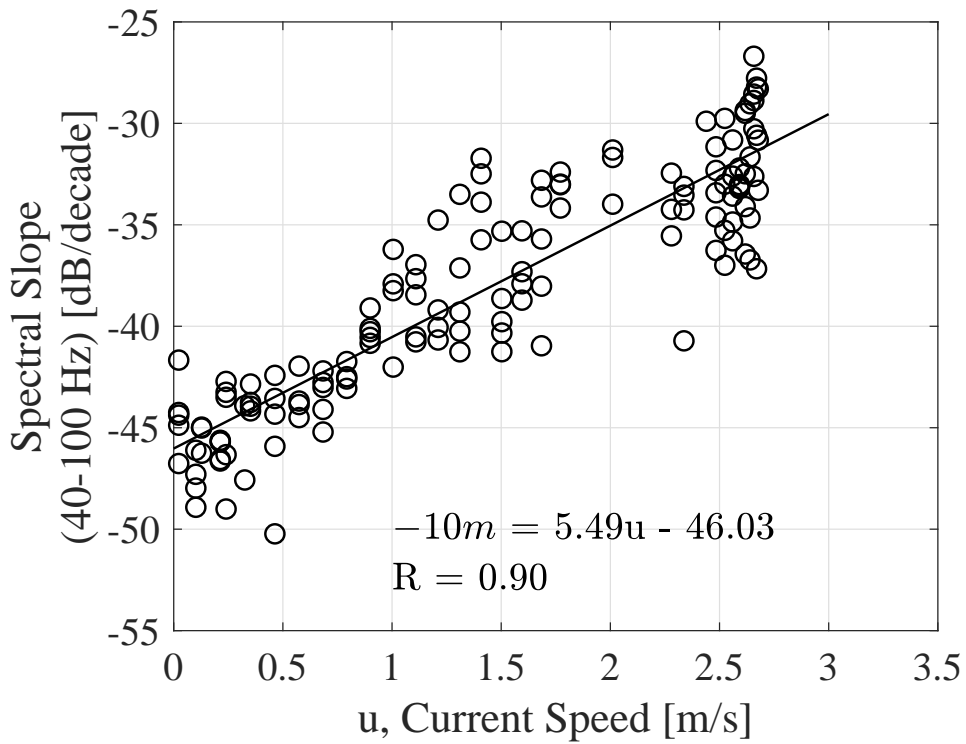


Fig. 3. Relationship between spectral slope,  $m$ , and current speed,  $u$ , between 40 and 100 Hz for channel 0. Spectral slope magnitude increases with decreasing flow. The correlation coefficient,  $R$ , is reported.

267 the tow body. If this were a moored system with no surface expression, that assumption might be valid,  
268 but is not considered here.

#### 269 *D. Spatial Coherence*

270 Spatial coherence is calculated for different hydrophone combinations across the linear array using  
271 (3). The spatial coherence results are presented in magnitude coherence for the entire deployment period  
272 (Fig. 5). If the wavelength of propagating sound is sufficiently long (frequency sufficiently low) the  
273 sensors would become relatively co-located and the coherence would tend to unity. However, the results  
274 suggest that the low frequency data is overwhelmingly incoherent, since the locally generated flow noise  
275 is incoherent from one hydrophone to the next.

276 Flow noise is uncorrelated and propagating ambient noise is highly correlated at low frequencies. As  
277 a result, low coherence and high coherence are a sign of flow noise and ambient noise, respectively.  
278 Therefore, the spatial coherence results are partitioned into two distinct regions: a flow noise region  
279 and an ambient noise region. Visual assessment suggests that flow noise is consistently present at low  
280 frequencies and can be prominent at higher frequencies (above 600 Hz). The ambient noise region is  
281 present between 200 and 600 Hz and contains the same vessel noise identified in Fig. 2.

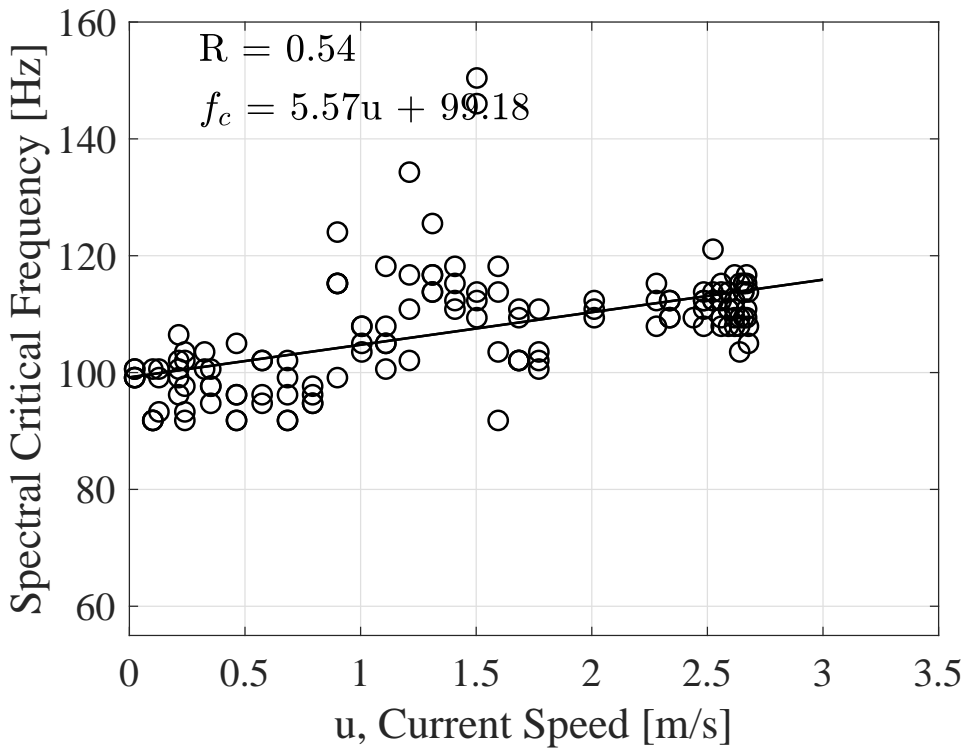


Fig. 4. Relationship between spectral critical frequency,  $f_c$ , and current speed,  $u$ , for channel 0. Spectral critical frequency marks where the flow noise and ambient noise contributions to the recorded signal are equal, and increases with current speed. Correlation coefficients,  $R$ , are reported.

#### 282 E. Coherence Critical Frequency

283 The coherence critical frequency is the highest frequency at which flow noise can be detected. The  
 284 coherence critical frequency was calculated for each minute of deployment for each combination of chan-  
 285 nels, and is used to quantify the relative prevalence of flow noise and ambient noise within a measurement  
 286 (Fig. 6). The coherence critical frequency is a more sensitive method of flow noise measurement than  
 287 the spectral critical frequency, as spatial coherence is used as an indicator of flow noise cessation rather  
 288 than relative noise contributions. The coherence critical frequency increases with increasing flow speed,  
 289 a relationship similar to that of the spectral critical frequency.

290 It is important to note that the coherence is impacted by any temporary deterministic noises present in  
 291 the sound field, such as the auxiliary RHIB, mechanical array noise, or noise generated aboard the *MV*  
 292 *Nova Endeavour*. In such instances, the automated coherence critical frequency detector fails, and yields  
 293 an outlier. These outliers have been removed.

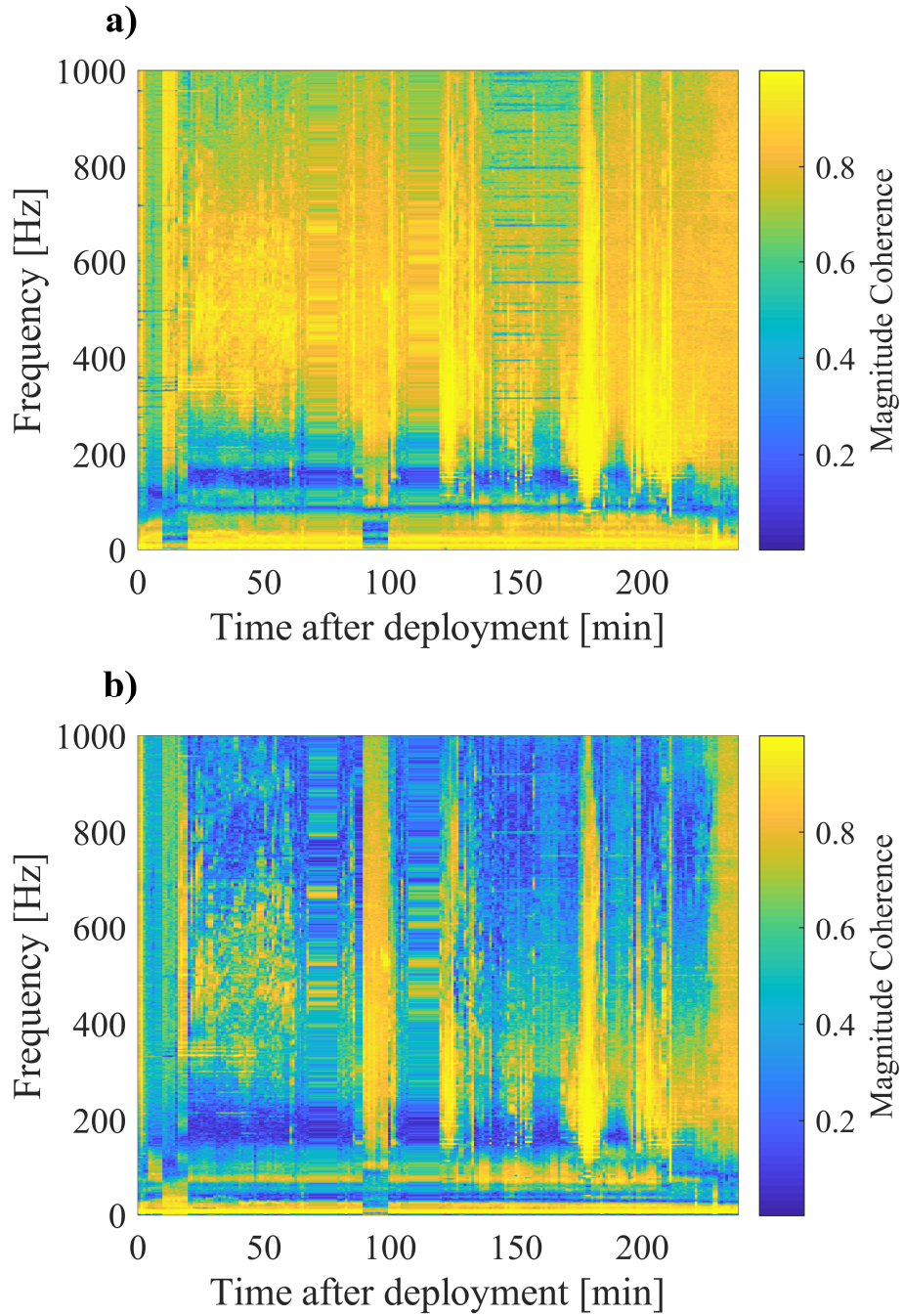


Fig. 5. Spatial coherence over the experimental period. Magnitude coherence is expected to tend to unity as the fixed hydrophones become relatively co-located. However, uncorrelated flow noise on each phone breaks that relationship. The extent of incoherent flow noise increases with current speed. Channel 0 - 1 (a) and 0 - 3 (b) are shown as examples. Results hold to all other channel combinations.

294 *F. Beamforming*

295 The spectral critical frequency of the coherent array output is compared to the fixed single hydrophone  
 296 spectral and coherence critical frequencies in Fig. 7. The standard deviations of the spectral slope and

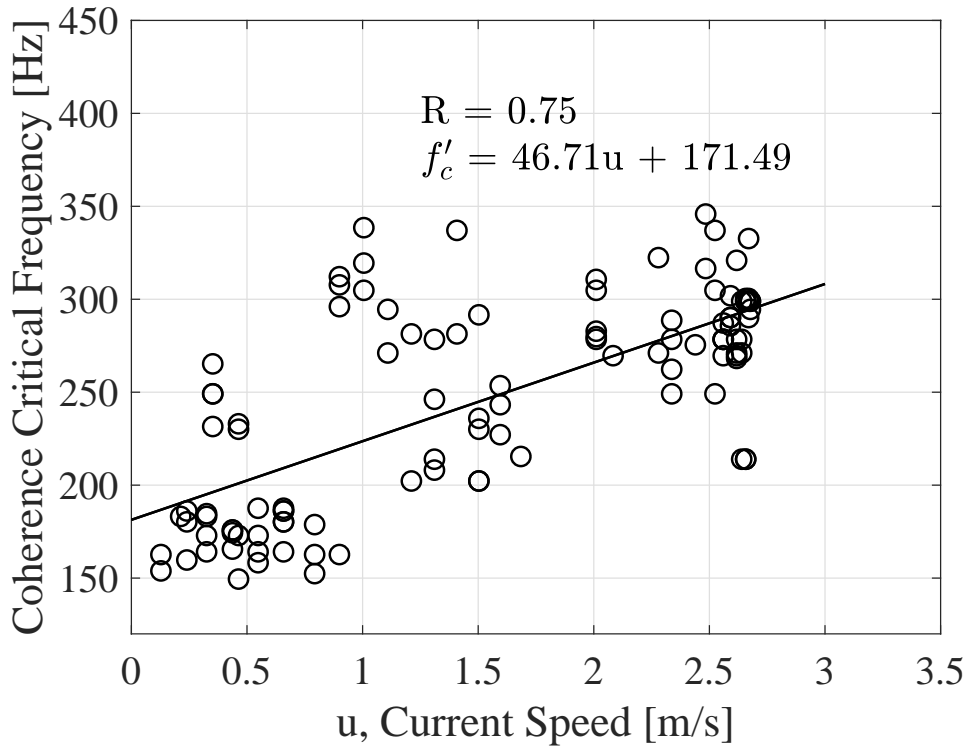


Fig. 6. Relationship between coherence critical frequency,  $f'_c$ , and current speed,  $u$ , for channels 0 - 1. Coherence critical frequency is the highest frequency at which flow noise can be detected, and increases with current speed.

297 spatial coherence critical frequency regressions were extracted from the averaged fits, while the standard  
298 deviation of the coherent array critical frequency regression was calculated from the data during the  
299 regression.

300 The coherence critical frequencies are relatively high, while spectral critical frequencies (both fixed  
301 single hydrophone and coherent array) are relatively low. This is attributed to the more sensitive nature  
302 of the coherence-based method. Above coherence critical frequencies we can be confident that there is  
303 no contamination of the ambient noise field by flow noise. Conversely, the fixed single hydrophone and  
304 coherent array spectral critical frequencies show where flow noise and ambient noise have equal power.  
305 The coherence and spectral critical frequencies serve as the respective upper and lower bounds of different  
306 noise regimes. Importantly, the coherent array output contains lower critical frequencies than the fixed  
307 single hydrophone, indicating that the broadside beamforming approach lessens the extent of flow noise  
308 within the measurements.

309 Fig. 8 compares GuardBuoy, fixed single hydrophone, and horizontal coherent array power spectra at  
310 1.5 hours into the experiment. We select a time where the drifter and array were in close proximity to  
311 establish a meaningful comparison.

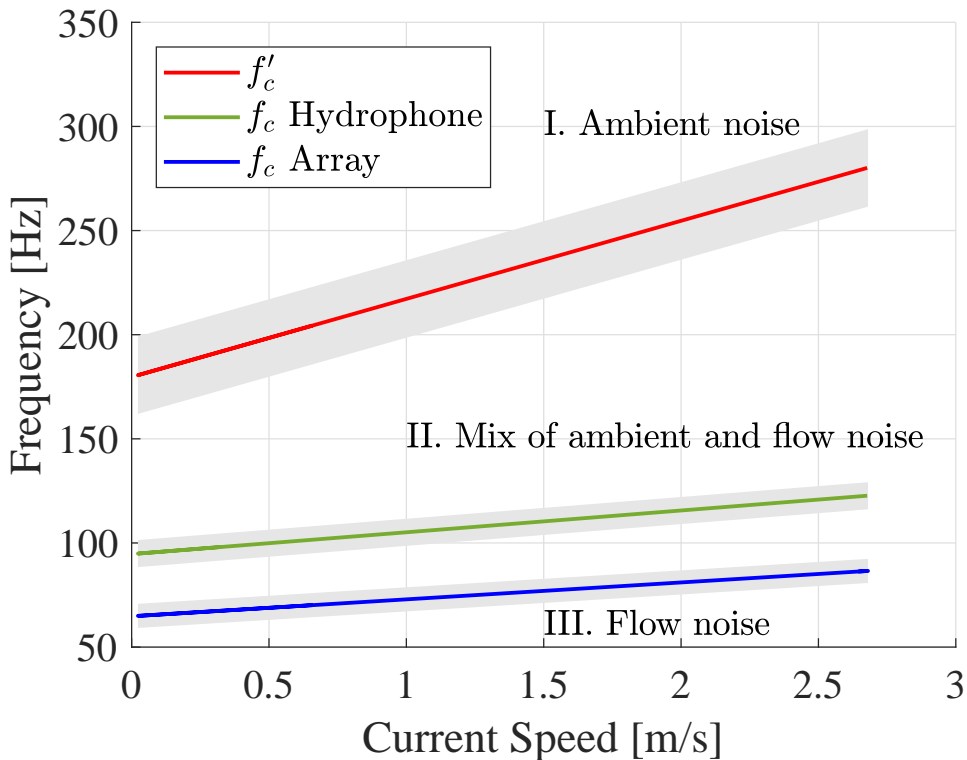


Fig. 7. Comparison of fixed single hydrophone spectral critical frequency (green), array spectral critical frequency (blue), and coherence critical frequency (red) as a function of current speed. Uncertainties are one standard deviation (shaded). Coherence critical frequency,  $f'_c$ , separates region I, where flow noise is negligible, and region II, where flow and ambient noise are both present, while spectral critical frequency,  $f_c$ , separates regions II and III, where flow noise dominates. The coherent array effectively suppresses flow noise, as indicated by its lower boundary relative to the fixed single hydrophone.

312 The GuardBuoy spectrum behaves differently from the rest, exhibiting lower levels at frequencies  
 313 below 100 Hz. A pronounced excursion in spectral slope is present at 10 Hz in the GuardBuoy spectrum,  
 314 suggesting non-negligible flow noise is affecting the drifter's low-frequency measurements. This is typical  
 315 of all moored or free drifting passive acoustic systems that have a surface expression or subsurface float.  
 316 The fixed single hydrophone shows clear symptoms of flow noise at low frequencies.

317 The spectra reveal that the coherent array spectra transitions to the ambient noise region at lower  
 318 frequencies than the fixed single hydrophone. Furthermore, the coherent array signals are quieter than  
 319 the fixed single hydrophone signals at all low frequencies, demonstrating the effective suppression of  
 320 flow noise. There is reasonable agreement between the GuardBuoy and coherent array above the critical  
 321 frequency, with some difference above 700 Hz. This disparity is attributed to the lack of co-location  
 322 between the array and the GuardBuoy, as they are vertically and horizontally displaced relative to each  
 323 other.

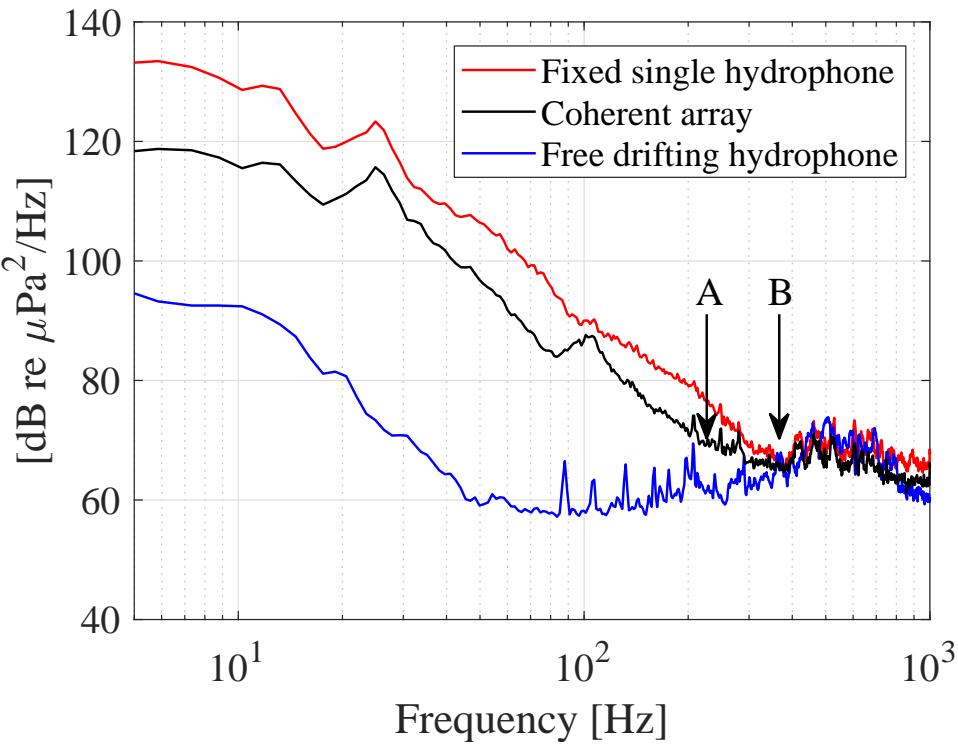


Fig. 8. Comparison of fixed single hydrophone (red), coherent array (black), and free drifting hydrophone (blue) signal power spectra at 1.5 hr into the deployment. The current speed at this moment was 2.2 m/s. A and B indicate the spectral critical frequencies of the coherent array and the fixed single hydrophone, respectively. The reduced levels and spectral critical frequency of the coherent array output relative to the fixed single hydrophone indicates effective flow noise suppression.

324

## V. DISCUSSION

### 325 A. Spectral Critical Frequency

326 Results show that critical frequency and flow speed are positively related, giving the intuitive result  
 327 that flow noise is prevalent in fast current conditions. The spectral critical frequency presents a method  
 328 of identifying flow noise prevalence within a signal.

329 The spectral critical frequency marks where ambient noise and flow noise have equal power, and  
 330 provides two important insights. Firstly, frequencies above the spectral critical frequency will contain a  
 331 mixture of ambient noise and flow noise. Secondly, frequencies below the spectral critical frequency will  
 332 be dominated by flow noise, since measurements in these frequencies contain spectral slopes that align  
 333 with turbulence theory. These insights are important, as they provide useful context for future signal level  
 334 and sound-source evaluations in tidal channel measurements.

335 *B. Spatial Coherence*

336 Spatial coherence results for different sensor combinations show that there are two distinct coherence  
 337 regions across the array: an incoherent flow noise region and a coherent ambient noise region. The  
 338 prevalence of these regions is quantified with the coherence critical frequency. Iterative calculations of the  
 339 coherence critical frequency were regressed against current speed. There is a positive relationship between  
 340 coherence critical frequency and current speed. The coherence critical frequency marks the frequency above  
 341 which flow noise is absent.

342 The spectral critical frequency provides a lower boundary, below which ambient noise is negligible,  
 343 and the coherence critical frequency provides an upper boundary, above which flow noise is negligible.  
 344 Frequencies between these bounds contain a mixture of flow noise and ambient noise. This explains why  
 345 the coherence critical frequencies are noticeably higher than those of the spectral method. The application  
 346 of spectral and coherence critical frequencies provides insight on the relative extent of both ambient noise  
 347 and flow noise within a signal.

348 *C. Beamforming*

349 By effectively treating the array as one sensor or hydrophone, signal processing can address the pseudo-  
 350 sound within low frequency data. Coherent averaging suppresses flow noise and enhances the detection of  
 351 propagating ambient noise. The coherent averaging employs a broadside approach with no steering angle  
 352 (19).

353 The results of the spectral critical frequencies derived from the beamformed array are shown in  
 354 Fig. 7. Evidently, the coherent array contains lower levels and lower critical frequencies than the fixed  
 355 single hydrophone (Fig. 7; Fig. 8). This implies that the coherent array is less affected by flow noise, and  
 356 contains a greater extent of ambient noise.

357 VI. CONCLUSION

358 Flow noise appears as:  $f^{-5/3}$  noise when wavelength  $\gg$  sensor size, and  $f^{-m}$  noise, where the sensor's  
 359 finite dimension reduces the flow noise.  $f^{-m}$  is related to the flow speed over the array. The spectral critical  
 360 frequency is used to identify where ambient noise is negligible and the coherence critical frequency is  
 361 used to identify where flow noise is negligible.

362 Coherent processing (beamforming) suppresses flow noise and yields a lower spectral critical frequency  
 363 than that of a fixed single hydrophone. An increased number of hydrophones and array length could  
 364 improve array performance.

365

## REFERENCES

- 366 [1] R. Karsten, A. Swan, and J. Culina, "Assessment of arrays of in-stream tidal turbines in the Bay of Fundy," *Phil. Trans. R. Soc. A*,  
 367 vol. 371, no. 1985, p. 20120189, 2013.
- 368 [2] R. Inger, M. J. Attrill, S. Bearhop, A. C. Broderick, W. James Grecian, D. J. Hodgson, C. Mills, E. Sheehan, S. C. Votier, M. J. Witt  
 369 *et al.*, "Marine renewable energy: potential benefits to biodiversity? An urgent call for research," *Journal of Applied Ecology*, vol. 46,  
 370 no. 6, pp. 1145–1153, 2009.
- 371 [3] M. J. Dadswell, "Occurrence and migration of fishes in Minas Passage and their potential for tidal turbine interaction," 2010.
- 372 [4] A. Redden and M. Stokesbury, "Acoustic tracking of fish movements in the Minas Passage and FORCE demonstration area: Pre-turbine  
 373 baseline studies (2011-2013)."
- 374 [5] D. Wang, M. Atlar, and R. Sampson, "An experimental investigation on cavitation, noise, and slipstream characteristics of ocean stream  
 375 turbines," *Proceedings of the Institution of Mechanical Engineers, Part A: Journal of Power and Energy*, vol. 221, no. 2, pp. 219–231,  
 376 2007.
- 377 [6] A. Lombardi, "Soundscape characterization in Grand Passage, Nova Scotia, a planned in-stream tidal energy site," 2016.
- 378 [7] M. K. Pine, A. G. Jeffs, and C. A. Radford, "Turbine sound may influence the metamorphosis behaviour of estuarine crab megalopae,"  
 379 *PLoS One*, vol. 7, no. 12, p. e51790, 2012.
- 380 [8] M. Halvorsen, T. Carlson, and A. Copping, "Effects of tidal turbine noise on fish," *PNNL Report-20787 for US Dept of Energy*, WA,  
 381 DC: by Pacific Northwest National Laboratory, Sequim, WA, pp. 1–41, 2011.
- 382 [9] M. Lighthill, "The Bakerian lecture, 1961. Sound generated aerodynamically," in *Proceedings of the Royal Society of London A:  
 383 Mathematical, Physical and Engineering Sciences*, vol. 267, no. 1329. The Royal Society, 1962, pp. 147–182.
- 384 [10] M. Strasberg, "Nonacoustic noise interference in measurements of infrasonic ambient noise," *The Journal of the Acoustical Society of  
 385 America*, vol. 66, no. 5, pp. 1487–1493, 1979.
- 386 [11] M. Van Dyke, *An album of fluid motion*. Parabolic Press Stanford, 1982, vol. 176.
- 387 [12] V. O. Knudsen, R. Alford, and J. Emling, "Underwater ambient noise," *J. Mar. Res.*, vol. 7, pp. 410–429, 1948.
- 388 [13] C. Bassett, J. Thomson, P. H. Dahl, and B. Polagye, "Flow-noise and turbulence in two tidal channels," *The Journal of the Acoustical  
 389 Society of America*, vol. 135, no. 4, pp. 1764–1774, 2014.
- 390 [14] D. R. Barclay and M. J. Buckingham, "Depth dependence of wind-driven, broadband ambient noise in the Philippine Sea," *The Journal  
 391 of the Acoustical Society of America*, vol. 133, no. 1, pp. 62–71, 2013.
- 392 [15] F. Dupont, C. G. Hannah, and D. Greenberg, "Modelling the sea level of the upper Bay of Fundy," *Atmosphere-Ocean*, vol. 43, no. 1,  
 393 pp. 33–47, 2005.
- 394 [16] B. Wilson, R. S. Batty, and L. M. Dill, "Pacific and atlantic herring produce burst pulse sounds," *Proceedings of the Royal Society of  
 395 London B: Biological Sciences*, vol. 271, no. Suppl 3, pp. S95–S97, 2004.
- 396 [17] J. A. Hildebrand, "Anthropogenic and natural sources of ambient noise in the ocean," *Marine Ecology Progress Series*, vol. 395, pp.  
 397 5–20, 2009.
- 398 [18] N. D. Merchant, T. R. Barton, P. M. Thompson, E. Pirotta, D. T. Dakin, and J. Dorocicz, "Spectral probability density as a tool for  
 399 ambient noise analysis," *The Journal of the Acoustical Society of America*, vol. 133, no. 4, pp. EL262–EL267, 2013.

- 400 [19] M. J. Buckingham, "On the two-point cross-correlation function of anisotropic, spatially homogeneous ambient noise in the ocean and  
401 its relationship to the Green's function," *The Journal of the Acoustical Society of America*, vol. 129, no. 6, pp. 3562–3576, 2011.
- 402 [20] B. F. Cron and C. H. Sherman, "Spatial-correlation functions for various noise models," *The Journal of the Acoustical Society of*  
403 *America*, vol. 34, no. 11, pp. 1732–1736, 1962.
- 404 [21] G. B. Deane, M. J. Buckingham, and C. T. Tindle, "Vertical coherence of ambient noise in shallow water overlying a fluid seabed,"  
405 *The Journal of the Acoustical Society of America*, vol. 102, no. 6, pp. 3413–3424, 1997.
- 406 [22] H. Cox, "Line array performance when the signal coherence is spatially dependent," *The Journal of the Acoustical Society of America*,  
407 vol. 54, no. 6, pp. 1743–1746, 1973.

408 **Matthew Auvinen** Biography text here.

PLACE  
PHOTO  
HERE

409

410 **David Barclay** Biography text here.

PLACE  
PHOTO  
HERE

411